PERFORMANCE ANALYSIS OF 1D SCATTERING CENTER EXTRACTION FROM WIDEBAND RADAR MEASUREMENTS

Zhou Jianxiong, Zhao Hongzhong, Shi Zhiguang, Fu Qiang

ATR Lab, National University of Defence Technology, Changsha, Hunan, China. 410073.

ABSTRACT

Performance bounds on the estimates of position, intensity and geometry parameter of scattering centers based on wideband radar measurements are presented in analytic forms. The resolution limit for wideband radar and the SNR threshold for identifying scatterer's geometry are further deduced. Though the results are obtained from the Cramér-Rao Bound (CRB) matrix for damped exponentials (DE) after simplification, their validity and adaptability for geometric theory of diffraction (GTD) based scattering data have been verified by simulations.

1. INTRODUCTION

Radar targets at high frequencies can be well characterized by a few scattering centers. Usually the scattering centers are extracted from wideband radar measurements by spectrum analysis methods. The estimation accuracy and their relation to radar/target arguments such as SNR, bandwidth, center frequency, etc., are of great interest in radar design and evaluation. The Cramér–Rao Bounds (CRB) for scattering models have been derived in previous literatures [1]-[3] but theses results are in high dimensional matrices difficult to simplify. Therefore the conclusions are always drawn from numerical calculations or Monte Carlo simulations, where the effects of different arguments are tested separately and no general conclusions can be obtained theoretically.

This problem is solved in this paper for well-separated scattering centers and two closely spaced scattering centers by simplifying the CRB matrix. The resolution limit and the SNR threshold for identifying geometry parameters are further deduced. These expressions explain and verify previous results [1]-[4] theoretically.

The simplification in this paper is based on the CRB for Damped Exponentials (DE), which is an approximation of Geometric Theory of Diffraction (GTD) model but is much easier to solve. Since DE model retains all the variables in GTD model, the CRB for these two models are close and the final results for DE model are applicable to GTD data, as will be verified by simulations. Similar simplifications have been done for Undamped Exponentials (UE) [5] which can also be used as scattering model but the geometry parameters are dropped. Since different variables are assumed in DE and UE, the final results for these two models differ greatly.

The paper is organized as follows. Section II reviews GTD and DE model briefly. Section III presents the simplification of the CRB matrix for DE model with physical significance and deduces further conclusions on the resolution limit and the geometry identifying threshold. These conclusions are verified by simulations in section IV.

2. 1D SCATTERING CENTER MODEL

GTD model describes the backscattered field of a perfectly conducted target at high frequencies by [1]:

$$E(f)=\sum_{m=1}^{M}A_m(\frac{f}{f_0})^{\alpha_m}e^{-j4\pi fr_m/c} \tag{1}$$

where the $e^{j2\pi ft}$ time convention is omitted and only one polarization channel is considered. The backscattered field mainly comes from M scattering centers with A_m the complex scattering coefficient at frequency f_0 and r_m the radial position of the mth scattering center; $(f/f_0)^{\alpha m}$ shows the amplitude dependence on frequency, where the geometry parameter α_m is decided by the scatterer's local geometric feature.

For wideband radar, the scattering data at N discrete frequencies can be written as:

$$s_{GTD}(n)=E(f_0+n\Delta f)=\sum_{m=1}^{M}a_m(1+n\frac{\Delta f}{f_0})^{\alpha_m}e^{jn\omega_m} \tag{2}$$

where

$$a_m=A_m\cdot e^{-j4\pi f_0r_m/c},\ \omega_m=-4\pi\Delta fr_m/c\ . \tag{3}$$

Usually f_0 is the center frequency, so the data is indexed symmetrically, i.e., n=–(N–1)/2,…,(N–1)/2 (N is odd) or n=–N/2+1,…,N/2 (N is even); Δf is the frequency step. Other radar arguments include bandwidth B, relative bandwidth γ and Fourier bin δr:

$$B=N\cdot\Delta f \tag{4a}$$

$$\gamma=N\Delta f/f_0=B/f_0 \tag{4b}$$

$$\delta r=\frac{c}{2B}\ . \tag{4c}$$

The power function in (2) can be approximated by exponential function to facilitate the estimation problem:

$$(1+n\frac{\Delta f}{f_0})^{\alpha_m} \approx \exp(\alpha_m \cdot n\frac{\Delta f}{f_0}) \text{ when } \left|n\frac{\Delta f}{f_0}\right| \ll 1 \cdot \quad (5)$$

Then GTD model is approximated by DE model:

$$s_{DE}(n) = \sum_{m=1}^{M} a_m e^{n\alpha_m \Delta f / f_0} \cdot e^{jn\omega_m} \triangleq \sum_{m=1}^{M} a_m z_m^n \quad (6)$$

where

$$z_m = p_m e^{j\omega_m} \ , \quad p_m = e^{\alpha_m \Delta f / f_0} \ . \quad (7)$$

DE model is also used in many other applications and its estimation problem is well solved.

3. PERFORMANCE ANALYSIS

3.1. Simplification of the CRB Matrix for DE Model

The data are assumed to be contaminated by white Gaussian noise $v(n)$ with variance σ^2:

$$x(n) = s_{DE}(n) + v(n) = \sum_{m=1}^{M} a_m z_m^n + v(n) \quad (8)$$

The complex parameter a_m and z_m contains two real parameters each:

$$a_m = |a_m| e^{j\varphi_m} \ , \quad z_m = p_m e^{j\omega_m} \ . \quad (9)$$

Suppose M is determined beforehand, the parameters to be estimated are:

$$\boldsymbol{\theta} = [\sigma^2 : \boldsymbol{\theta}_{|a|}^T : \boldsymbol{\theta}_{\varphi}^T : \boldsymbol{\theta}_{p}^T : \boldsymbol{\theta}_{\omega}^T]^T \quad (10)$$

where $\boldsymbol{\theta}_{aR}=[|a_1|,\ldots,|a_M|]^T$, $\boldsymbol{\theta}\varphi=[\varphi_1,\ldots,\varphi_M]^T$, $\boldsymbol{\theta}_P=[p_1,\ldots,\ p_M]^T$, $\boldsymbol{\theta}_\omega=[\omega_1,\ldots,\ \omega_M]^T$. The CRB matrix for DE model is [3]:

$$\mathrm{CRB}_{\boldsymbol{\theta}} = \begin{bmatrix} \frac{\sigma^4}{N} & \mathbf{0}_{1\times 4M} \\ \mathbf{0}_{4M\times 1} & \frac{\sigma^2}{2}\mathbf{F} \end{bmatrix} \quad (11)$$

where $\mathbf{F}$ is given in (12) at the bottom of this page where $\overline{\ }$ and $\widetilde{\ }$ stands for the real and imaginary part respectively. $\boldsymbol{\Phi}$=diag($e^{j\varphi_1}$, $e^{j\varphi_2}$,…, $e^{j\varphi_M}$), $|\mathbf{A}|$=diag($|a_1|,|a_2|,\ldots,|a_M|$), $\mathbf{P}$=diag($p_1,p_2,\ldots,p_M$), $\mathbf{N}$=diag($n_0,n_0+1,\ldots,n_0+N-1$) with $n_0 = \begin{cases} -(N-1)/2, & N \text{ odd} \\ -N/2+1, & N \text{ even} \end{cases}$, $\mathbf{E}=(\mathbf{Z}^H\mathbf{Z})^{-1}$, $\mathbf{Q}=\mathbf{B_2}-\mathbf{BEB}$, $\mathbf{B}=\mathbf{Z}^H\mathbf{N}\mathbf{Z}$, $\mathbf{B_2}=\mathbf{Z}^H\mathbf{N}^2\mathbf{Z}$, $\mathbf{Z}=[\mathbf{z}_1,\mathbf{z}_2,\ldots,\mathbf{z}_M]$, $\mathbf{z}_m={z_m}^{n_0}[1,z_m,\ldots,{z_m}^{N-1}]^T$ with m=1,…,M.

Approximations and constraints will be used to derive the simplified expressions for the diagonal elements in the CRB matrix. For a common radar system we assume p_m=1 since $\Delta f/f_0$<<1 and the adaptability for p_m≈1 will be tested by simulations. And only the special case for M=1 and M=2 are considered in the derivation.

The one component case (M=1) is applicable when the interference between adjacent components is negligibly small. For radar targets, it means that the adjacent scattering centers are well separated, e.g., their interval is larger than two Fourier bins, as will be demonstrated later.

In this case $\mathbf{E}=\frac{1}{N}$, $\mathbf{B}=o(N^2)$, $\mathbf{B_2}=\frac{N^3}{12}+o(N^2)$, $\mathbf{Q}=\frac{N^3}{12}+o(N^2)$, where N>10 is assumed and $o(\cdot)$ denotes higher order minimal. Omitting the higher order terms in (12), we obtain

$$\frac{1}{|a|^2}CRB_{|a|} = CRB_{\varphi} \approx \frac{\sigma^2}{2N|a|^2}, \ \frac{1}{p^2}\cdot CRB_p = CRB_{\omega} \approx \frac{6\sigma^2}{|a|^2 N^3} \quad (13)$$

In the two component case (M=2), $p_1=p_2=1$, $z_1=e^{j\omega_1}$, $z_2=e^{j\omega_2}$. Let $\Delta\omega=\omega_2-\omega_1$ and $\Omega=N\Delta\omega$, we can prove that the 2×2 matrices $\mathbf{E}$, $\mathbf{B}$, $\mathbf{B_2}$, $\mathbf{Q}$ are proportional to $1/N$, N^2 N^3 and N^3 respectively and their elements are functions of Ω if omitting the higher order terms. Applying these properties to (12), we obtain:

$$\frac{1}{|a_m|^2}CRB_{|a_m|} = CRB_{\varphi_m} \approx \frac{\sigma^2}{2N|a_m|^2}\cdot r_a(\Omega) \quad (14a)$$

$$\frac{1}{{p_m}^2}\cdot CRB_{p_m} = CRB_{\omega_m} \approx \frac{\sigma^2}{2|a_m|^2 N^3}\cdot r_\omega(\Omega) \quad (14b)$$

where r_a and r_ω are undetermined coefficients. We obtain their functional relation by numerical fitting as in Fig.1.

The functional relations of r_a~Ω (solid line) and r_ω~Ω (dashed line) for four different N values are calculated straightforwardly using (12) and the N-independent approximations (omitting the higher order terms) are marked by '+'. Fig.1 shows that: ①The curves for different N and the N-independent approximation coincide on the whole. ② $r_a\to 1$ and $r_\omega\to 12$ when $\Omega>>2\pi$, i.e., (14) approaches (13); and the limit is well achieved when $\Omega\geq 4\pi$. ③When $\Omega\leq 2\pi$, the curves for r_a~Ω and r_ω~Ω are linear in logarithmic coordinates. Therefore the original function can be approximated by power function:

$$r_a \approx K_a \cdot \Omega^{-6.30}, \quad r_\omega \approx K_\omega \cdot \Omega^{-4} \quad (\Omega \leq 2\pi) \quad (15)$$

where K_a≈4.04×10^5, K_ω≈1.07×10^5.

Now we obtain the analytic CRB expressions in the two component case when $\Omega\leq 2\pi$:

$$\mathbf{F} = \begin{bmatrix} \overline{\boldsymbol{\Phi}^H(\mathbf{E}+\mathbf{EBQ}^{-1}\mathbf{BE})\boldsymbol{\Phi}} & -\widetilde{\boldsymbol{\Phi}^H(\mathbf{E}+\mathbf{EBQ}^{-1}\mathbf{BE})\boldsymbol{\Phi}}\,|\mathbf{A}|^{-1} & -\overline{\boldsymbol{\Phi}^H\mathbf{EBQ}^{-1}\boldsymbol{\Phi}}\,|\mathbf{A}|^{-1}\,\mathbf{P} & \widetilde{\boldsymbol{\Phi}^H\mathbf{EBQ}^{-1}\boldsymbol{\Phi}}\,|\mathbf{A}|^{-1} \\ |\mathbf{A}|^{-1}\,\widetilde{\boldsymbol{\Phi}^H(\mathbf{E}+\mathbf{EBQ}^{-1}\mathbf{BE})\boldsymbol{\Phi}} & |\mathbf{A}|^{-1}\,\overline{\boldsymbol{\Phi}^H(\mathbf{E}+\mathbf{EBQ}^{-1}\mathbf{BE})\boldsymbol{\Phi}}\,|\mathbf{A}|^{-1} & -|\mathbf{A}|^{-1}\,\widetilde{\boldsymbol{\Phi}^H\mathbf{EBQ}^{-1}\boldsymbol{\Phi}}\,|\mathbf{A}|^{-1}\,\mathbf{P} & -|\mathbf{A}|^{-1}\,\overline{\boldsymbol{\Phi}^H\mathbf{EBQ}^{-1}\boldsymbol{\Phi}}\,|\mathbf{A}|^{-1} \\ -\mathbf{P}\,|\mathbf{A}|^{-1}\,\overline{\boldsymbol{\Phi}^H\mathbf{Q}^{-1}\mathbf{BE}\boldsymbol{\Phi}} & \mathbf{P}\,|\mathbf{A}|^{-1}\,\widetilde{\boldsymbol{\Phi}^H\mathbf{Q}^{-1}\mathbf{BE}\boldsymbol{\Phi}}\,|\mathbf{A}|^{-1} & \mathbf{P}\,|\mathbf{A}|^{-1}\,\overline{\boldsymbol{\Phi}^H\mathbf{Q}^{-1}\boldsymbol{\Phi}}\,|\mathbf{A}|^{-1}\,\mathbf{P} & -\mathbf{P}\,|\mathbf{A}|^{-1}\,\widetilde{\boldsymbol{\Phi}^H\mathbf{Q}^{-1}\boldsymbol{\Phi}}\,|\mathbf{A}|^{-1} \\ -|\mathbf{A}|^{-1}\,\widetilde{\boldsymbol{\Phi}^H\mathbf{Q}^{-1}\mathbf{BE}\boldsymbol{\Phi}} & -|\mathbf{A}|^{-1}\,\overline{\boldsymbol{\Phi}^H\mathbf{Q}^{-1}\mathbf{BE}\boldsymbol{\Phi}}\,|\mathbf{A}|^{-1} & |\mathbf{A}|^{-1}\,\widetilde{\boldsymbol{\Phi}^H\mathbf{Q}^{-1}\boldsymbol{\Phi}}\,|\mathbf{A}|^{-1}\,\mathbf{P} & |\mathbf{A}|^{-1}\,\overline{\boldsymbol{\Phi}^H\mathbf{Q}^{-1}\boldsymbol{\Phi}}\,|\mathbf{A}|^{-1} \end{bmatrix} \quad (12)$$

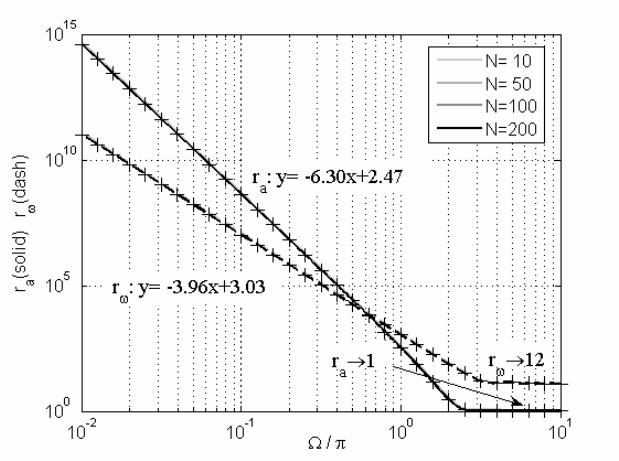

Fig.1. r_a and r_ω versus Ω

$$\frac{1}{|a_m|^2} CRB_{|a_m|} = CRB_{\varphi_m} \approx \frac{\sigma^2 K_a}{2N|a_m|^2} \Omega^{-6.3} \quad (\Omega \le 2\pi) \quad (16a)$$

$$\frac{1}{p_m^2} \cdot CRB_{p_m} = CRB_{\omega_m} \approx \frac{\sigma^2 K_\omega}{2|a_m|^2 N^3} \Omega^{-4} \quad (\Omega \le 2\pi) \quad (16b)$$

When $\Omega \ge 4\pi$, the CRB for each component can be well evaluated by (13). When $2\pi < \Omega < 4\pi$ we can predict the CRB to be between that of (13) and (16) but can not obtain simple analytic expressions to describe it.

Though we have only simplified the CRB for DE model in the one or two component case, the results are applicable to the well separated components (result (13)) and the closely spaced two components (result (16)) in multiple component case. However, if more than two components are closely spaced, the CRB will be worse than the two component case because of more interference, as has been verified by numerical calculations. Therefore (16) provides a lower limit in this case.

3.2. Performance Bounds for 1D Scattering Center Extraction

The scattering parameters in (1) can be estimated from the mathematic parameters in (8):

$$\hat{r}_m = -\frac{c}{4\pi\Delta f} \cdot \hat{\omega}_m, \quad \hat{\alpha}_m = \frac{f_0}{\Delta f} \cdot \ln \hat{p}_m, \quad \hat{A}_m = \hat{a}_m \cdot e^{j4\pi f_0 \hat{r}_m / c} \quad (17)$$

The estimation error is passed to the scattering parameters so that

$$\mathrm{var}\{\hat{r}_m\} = \frac{c^2}{(4\pi)^2 \Delta f^2} \cdot \mathrm{var}\{\hat{\omega}_m\} \quad (18a)$$

$$\mathrm{var}\{\hat{\alpha}_m\} = (\frac{f_0}{\Delta f})^2 \cdot \frac{1}{p_m^2} \mathrm{var}\{\hat{p}_m\} \quad (18b)$$

$$\mathrm{var}\{|\hat{A}_m|\} = \mathrm{var}\{|\hat{a}_m|\} \ . \quad (18c)$$

Hence the performance bounds for these scattering parameters can be deduced from (13) and (16), and some further results can be deduced from them. We define SNR_m in the image domain as the ratio of the peak signal power of the mth scattering center to the noise floor: $SNR_m = \frac{N|a_m|^2}{\sigma^2}$.

For position estimates:

$$\mathrm{var}\{\hat{\bar{r}}_m\} \ge \frac{3}{2\pi^2} \cdot \frac{1}{SNR_m} \quad (\Delta\bar{r} >> 1) \quad (19a)$$

$$\mathrm{var}\{\hat{\bar{r}}_m\} \ge \frac{K_\omega}{128\pi^6} \cdot \frac{1}{SNR_m} \cdot \Delta\bar{r}^{-4} \quad (\Delta\bar{r} \le 1) \quad (19b)$$

where $\bar{r}_m = r_m / \delta r$ is the normalized position and $\Delta\bar{r} \triangleq \Delta r / \delta r = \Omega/(2\pi)$ is the normalized interval; Δr is the smaller between $|r_m - r_{m-1}|$ and $|r_{m+1} - r_m|$; δr is the Fourier bin defined in (4c). The condition $\Delta\bar{r} >> 1$ is thought to be satisfied when $\Delta\bar{r} \ge 2$, as have been explained before. When $1 < \Delta\bar{r} < 2$ the performance bounds will be between (19a) and (19b). This property holds for similar equations in the following.

When two scattering centers are closely spaced with normalized interval $\Delta\bar{r}$ ($\Delta\bar{r} \le 1$), they may be resolved by superresolution algorithms if $\mu\sqrt{\mathrm{var}\{\hat{\bar{r}}_m\}} \le \frac{\Delta\bar{r}}{2}$ where μ determines the probability of resolving, e.g., μ=3 implies a resolving probability of 99.7% when $\hat{\bar{r}}_m$ is normally distributed. The resolution limit can then be deduced to be:

$$\Delta\bar{r}_{\lim} \ge \frac{(2\mu^2 \cdot K_\omega)^{1/6}}{2\pi} \cdot SNR_m^{-1/6} \quad (20)$$

where m denotes the one with lower SNR between the two adjacent scattering centers.

This relation has been studied in [1], [3], [4] by numerical calculations but no general expressions have been obtained. Comparing with the expressions in [5], we see that the resolution limit for DE is similar to that for UE at the worst (phase) condition. This is intuitive since the DE model has less prior information than the UE model.

For geometry parameter estimates:

$$\mathrm{var}\{\hat{\alpha}_m\} \ge (\frac{f_0}{\Delta f})^2 \cdot \frac{6\sigma^2}{|a_m|^2 N^3} = \frac{6}{\gamma^2 \cdot SNR_m} \quad (\Delta\bar{r} >> 1) \quad (21a)$$

$$\mathrm{var}\{\hat{\alpha}_m\} \ge \frac{K_\omega}{32\pi^4} \cdot \frac{1}{\gamma^2 \cdot SNR_m} \cdot \Delta\bar{r}^{-4} \quad (\Delta\bar{r} \le 1) \quad (21b)$$

where γ is the relative bandwidth defined in (4b). Equation (21) shows that increasing relative bandwidth is the most effective way to improve the estimation accuracy of geometry parameter. This has been proposed in [1], [2], [4], whereas (21) provides a theoretical evidence.

Since the geometry parameters are discrete values from $\{-1, -0.5, 0, 0.5, 1\}$ for most strong scattering centers, identifying it demands $\mu\sqrt{\mathrm{var}\{\hat{\alpha}_m\}} < 0.25$ where μ determines the probability of identifying. Therefore the SNR threshold for correctly identifying scatterer's geometry is:

$$SNR_m \ge \frac{96\mu^2}{\gamma^2} \quad (\Delta\bar{r} >> 1) \quad (22a)$$

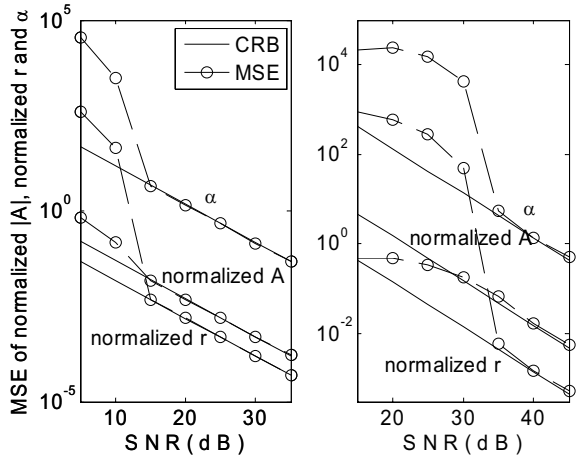

Fig.2. MES of scattering center parameter estimation in case 1 (left) and case 2 (right).

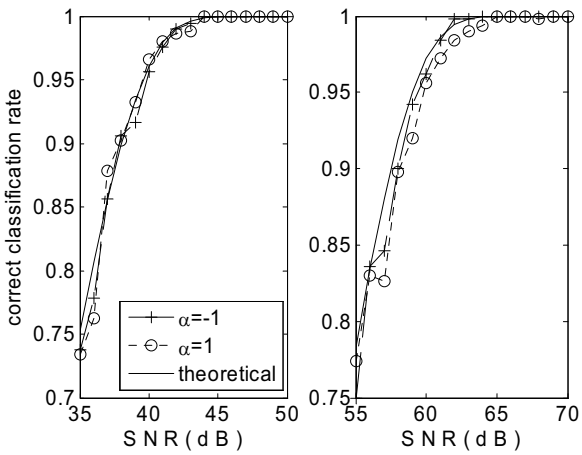

Fig.3. Identifying rate of geometry parameter in case 1 (left) and case 2 (right).

$$SNR_m \geq \frac{\mu^2 K_\omega}{2\pi^4 \gamma^2} \cdot \Delta\bar{r}^{-4} \quad (\Delta\bar{r} \leq 1). \tag{22b}$$

For intensity estimates:

$$\mathrm{var}\{\left|\hat{\bar{A}}_m\right|\} = \frac{\mathrm{var}\{\left|\hat{A}_m\right|\}}{\left|a_m\right|^2} \geq \frac{\sigma^2}{2N\left|a_m\right|^2} = \frac{1}{2SNR_m} \quad (\Delta\bar{r} >> 1) \tag{23a}$$

$$\mathrm{var}\{\left|\hat{\bar{A}}_m\right|\} \geq \frac{K_a}{2\cdot(2\pi)^{6.3}} \cdot \frac{1}{SNR_m} \cdot \Delta\bar{r}^{-6.3} \quad (\Delta\bar{r} \leq 1). \tag{23b}$$

where $\bar{A}_m$ is the normalized intensity whose true value is 1. Comparing (23b) with (21b) and (19b) we see that for closely spaced scattering centers, the variance of intensity estimates grows much faster than that of position or geometry estimates with the decrease of the normalized interval.

4. NUMERICAL EXAMPLES

The data are generated by GTD model in (2). Radar arguments are f_0=10GHz, Δf=20MHz, N=101. In all the experiments, the number of scattering centers is assumed to be known. The STLN algorithm [6] is used for parameter estimation.

We test the estimation performance of the scattering parameters at different SNR levels for well separated scattering centers (case 1) and adjacent scattering centers (case 2). Target arguments are set as M=2, A_1=A_2=1, r_1=1m, r_2=−1m, α_1=1, α_2=−1 in case 1 and M=2, A_1=$e^{j\varphi_1}$, A_2= $e^{j\varphi_2}$ (φ_1 and φ_2 are randomly generated in each trial to avoid the fixed effects of phase on estimators [7]), r_1=0, r_2=0.0375m, α_1=1, α_2=−1 in case 2. 500 trials are performed and the mean square error is averaged over the two scattering centers in Fig.2. We see that the estimator can approach the theoretical bounds when the SNR exceeds a certain threshold. In case 1 the threshold is about 15dB and in case 2 it can be approximately decided by (20).

We also count the correct identifying rate of geometry parameters and compare it with the theoretical rate $\mathrm{R_{id}}=erf(\frac{1}{4\sqrt{2\mathrm{var}(\hat{\alpha})}})$ (where $erf(x)=\frac{2}{\sqrt{\pi}}\int_0^x e^{-t^2}dt$ is error function and $\hat{\alpha}$ is assumed to be unbiased and normally distributed with variance achieving the lower bound in (21)) in Fig.3. For the radar arguments in this simulation, the SNR threshold for identifying scatter's geometry is always 30dB higher than the working threshold in Fig.2. This hinders the utilization of geometry parameter in disadvantageous environment.

5. REFERENCES

[1] L. C. Potter, D.-M. Chiang, R. Carriere, and M. J. Gerry, "A GTD-based parametric model for radar scattering," *IEEE Trans. Antennas Propagat.*, vol. 43, pp. 1058-1067, Oct. 1995.

[2] M. J. Gerry, L. C. Potter, I. J. Gupta, and A. V. Merwe, "A parametric model for synthetic aperture radar measurements," *IEEE Trans. Antennas Propagat.*, vol. 47, pp. 1179–1188, July 1999.

[3] W. M. Steedly and R. L. Moses, "The Cramér-Rao bound for pole and amplitude estimates of damped exponential signals in noise," *IEEE Trans. Signal Processing*, vol.41, pp.1305-1318, Mar. 1993.

[4] M. McClure, R. C. Qiu, L. Carin, "On the superresolution identification of observables from swept-frequency scattering data," *IEEE Trans. Antennas Propagat.*, vol. 45, pp. 631-641, Apr. 1997.

[5] E. Dilaveroğlu, "Nonmatrix Cramér-Rao bound expressions for high-resolution frequency estimators," *IEEE Trans. Signal Processing*, vol.46, pp.463-474, Feb. 1998.

[6] B. De Moor, "Total least squares for affinely structured matrices and the noisy realization problem," *IEEE Trans. Signal Processing*, vol. 42, pp.3104-3113, Nov. 1994.

[7] D. M. Wilkes and J. A. Cadzow, "The effects of phase on high resolution frequency estimators," *IEEE Trans. Signal Processing*, vol.41, pp. 1319-1330, Mar. 1993.